# Self-Assembly of Light-Harvesting Crystalline Nanosheets in Aqueous Media

Chen Shahar,[†] Jonathan Baram,[†] Yaron Tidhar,[†] Haim Weissman,[†] Sidney R. Cohen,[‡] Iddo Pinkas,[‡] and Boris Rybtchinski[†,*]

Departments of [†]Organic Chemistry and [‡]Chemical Research Support, Weizmann Institute of Science, Rehovot 76100, Israel

ABSTRACT A methodology leading to facile self-assembly of crystalline aromatic arrays in dilute aqueous solutions would enable efficient fabrication and processing of organic photonic and electronic materials in water. In particular, soluble 2D crystalline nanosheets may mimic the properties of photoactive thin films and self-assembled monolayers, covering large areas with ordered nanometer-thick material. We designed such solution-phase arrays using hierarchical self-assembly of amphiphilic perylene diimides in aqueous media. The assemblies were characterized by cryogenic transmission electron microscopy (cryo-TEM), revealing crystalline order and 2D morphology (confirmed by AFM studies). The order and morphology are preserved upon drying as evidenced by TEM and AFM. The 2D crystalline-like structures exhibit broadening and red-shifted absorption bands in UV−vis spectra, typical for PDI crystals and liquid crystals. Photophysical studies including femtosecond transient absorption spectroscopy reveal that two of the assemblies are superior light-harvesters due to excellent solar spectrum coverage and fast exciton transfer, in one case showing exciton diffusion comparable to solid-state crystalline systems based on perylene tetracarboxylic dianhidride (PTCDA).
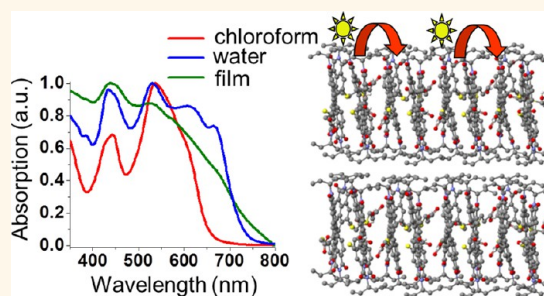
KEYWORDS: self-assembly · aromatic amphiphiles · 2D crystals · exciton diffusion · water · perylene diimides · energy transfer · photonic materials

Water can mediate unique self-assembly modes where simple building blocks form ordered nanoscale arrays with complex structures.[1−7] For example, complex and diverse structures, dendrimerosomes, were shown to self-assemble from relatively simple dendritic amphiphiles,[8] allowing an access to a new family of nanostructures in water. Aqueous self-assembly of simple polyalcohol-based amphiphiles such as glycerol mono-olein or phytantriol leads to cubosomes, ordered bicontinuous nanoarrays with cubic morphology and highly periodic structure.[4,9] However, rational design of such systems is extremely challenging, requiring better understanding of specific molecular interactions in water.[1,3,10] Controlling such interactions to create assemblies with crystalline order is highly desirable: *e.g.*, crystalline aromatic structures are core components of photonic and electronic devices, where key functions such as exciton and electron transfer critically depend on the molecular organization and degree of order.[11−14] Thus, rational design of self-assembled *crystalline aromatic arrays in dilute aqueous solutions* would enable efficient fabrication and processing of organic photonic and electronic materials in water. In particular, crystalline aromatics are capable of fast exciton transfer over long distances[13−16] that is of primary importance for efficient light harvesting in organic solar cells[17,18] and in artificial photosynthesis.[19] To overcome challenges related to fabrication of solid state crystalline materials, significant effort has been devoted to the design of solution-phase aromatic assemblies that efficiently transfer excitons.[20−22] In this respect, soluble aromatic arrays having crystalline order should be most effective. Particularly, soluble 2D crystalline nanosheets represent a very interesting target as they may mimic the properties of thin films and self-assembled monolayers, covering large areas with ordered nanometer-thick material. We note that rational design of organic crystals is a long-standing problem;[23−25] hence, encoding molecular interactions that lead to solution-phase crystalline systems may advance rational
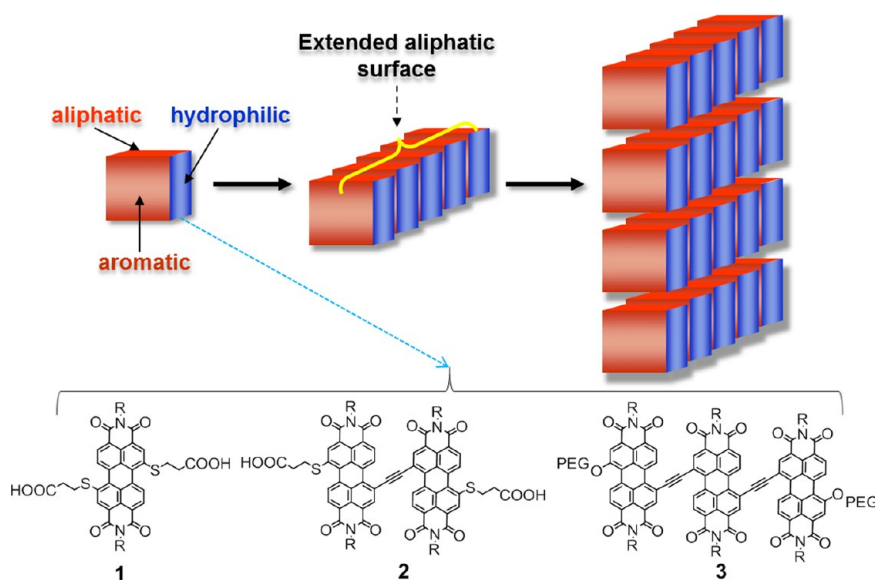
Figure 1. Illustration of the assembly formation (top), and structures of the molecular building blocks (bottom, R = ethyl propyl; PEG = $-CH_2CH_2(OCH_2CH_2)_{16}CH_3$).

design of organic crystals using aqueous self-assembly.

Here, we report on a rational design of 2D systems with crystalline-like structures having thickness of several nanometers that self-assemble in aqueous media from well-defined perylene diimide (PDI) amphiphiles. Two of the assemblies are superior light-harvesters: they exhibit excellent solar spectrum coverage and fast exciton transfer, in one case showing exciton diffusion comparable to solid-state crystalline systems.

RESULTS AND DISCUSSION

Design and Self-Assembly. Aromatic amphiphiles are capable of hierarchical interactions responsible for complex "nonclassical" assemblies in water.[6,8,26] We employ such hierarchical hydrophobic interactions to design ordered aromatic arrays. In the case of alkyl-bearing aromatic amphiphiles, if the hydrophobic/ $\pi-\pi$ interactions between the aromatic units are dominant and lead to formation of extended stacks, the latter develop new hydrophobic surfaces consisting of alkyls, which impose interaction between the stacks, a mode observed by us in some self-assembled nanofibers.[27−29] We envisaged that an amphiphile having a large aromatic core decorated with two alkyls and two hydrophilic groups may lead to an extended 1D stack motif with two newly formed hydrophobic alkyl surfaces (stack edges, Figure 1). These can connect the rigid 1D stacks leading to ordered 2D systems (the two hydrophilic groups of bolamphiphilic molecules limit the assembly growth in two dimensions). The crystalline systems are molecular monolayers, with cross sections corresponding to molecular dimensions (several nanometers for extended aromatic systems); thus, the choice of the aromatic amphiphile controls the thickness of the assembly. 2D crystalline

nanosheets in dilute aqueous solutions are rare, and in most cases are based on polymeric amphiphiles,[30,31] while light harvesting properties of such assemblies have not been investigated. In our study of metal-tuned hydrophobic self-assembly, we observed formation of a 2D nanocrystalline system assembled from PDI amphiphiles bearing terpyridine silver complexes.[28] In this array, metal coordination appears to play a key role in creating ordered assembly; furthermore, it was not predesigned based on primary building block structure, and was not amenable to photophysical studies due to photodegradation. In general, rational design approaches toward extended 2D crystalline assemblies based on small molecules in aqueous solutions have not been developed.

On the basis of the above-mentioned considerations, we synthesized compounds **1**−**3** (Figure 1) that have perylene diimide (PDI) cores functionalized with two alkyl groups (ethyl propyls attached at imide positions), and two hydrophilic groups (PEG or carboxyl, attached to the aromatic core). Compound **1** has a single PDI core bearing two ethyl propyl groups at imide positions and carboxylic acid groups attached to the aromatic core; **2** is an analog of **1**, having an extended bis-PDI core. We assumed that relatively compact carboxylic groups may favor the assembly motif presented in Figure 1. Compound **3** has bulkier hydrophilic PEGs counterbalanced by a larger hydrophobic core, seeking to extend the design strategy beyond small hydrophilic groups (see Supporting Information for synthesis and characterization of **1**−**3**). We note that PDI-based amphiphiles are excellent building blocks for a wide variety of self-assembled arrays in aqueous media, benefiting from high stability, diverse synthetic strategies, and advantageous photonic and electronic properties.[32] PDI amphiphiles
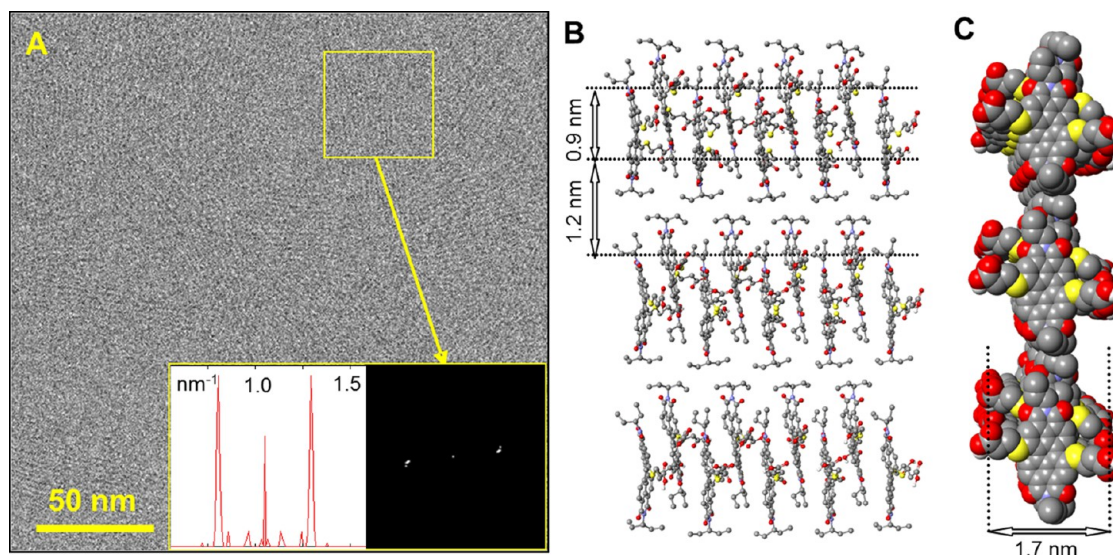
Figure 2. (A) Cryo-TEM image of 1×10^{-4} M solution of 1 in water (pH 5). Inset: FFT analysis of the marked area. (B,C) Molecular model (hydrogens are omitted for clarity): (B) interacting stacks and dimensions corresponding to the dark and light contrast stripes in the assemblies; (C) side view (space filling representation) showing the width of the assembly (monolayer cross-sectional view).

have recently been employed in functional water-based nanomaterials such as pH sensors/white light emitters,[33] recyclable filtration membranes,[34] and hybrid photoactive systems relevant to solar energy conversion.[35−37] In addition, controlled precipitation of PDI systems in protic solvents leads to highly ordered PDI fibers in the solid state.[38]

The self-assembly of compound 1 in water (pH 5) results in highly ordered arrays as evidenced by cryogenic transmission electron microscopy (cryo-TEM) (Figure 2A). The vitrified water areas are completely covered by arrays of uniformly spaced intermittent darker- and lighter-contrast stripes. Crystalline-like order of the assembly is evident from Fast Fourier Transform (FFT) analysis exhibiting well-defined spots corresponding to periodicity of 2.1 nm (Figure 2A). Cryo-TEM images reveal the dark contrast stripes having width of 1.0 ± 0.1 nm and the lighter contrast interstripe areas, 1.0 ± 0.3 nm in width (Figure 2; due to the insufficient contrast of the images, the measurements of individual dark and light features are less reliable than in the case of compounds 2 and 3 whose images have a higher contrast, see below). Similar assemblies were observed at basic conditions (pH 10, Supporting Information Figure S6). Molecular models that fit best the cryo-TEM data involve a crystalline monomolecular layer built from PDI stacks that interact via ethyl propyl groups (Figure 2B), in accordance with the model presented in Figure 1. The darker contrast stripes in cryo-TEM correspond to the overlapping aromatic cores (0.9 nm), and the lighter contrast ones to the ethyl propyl groups and parts of the nonoverlapping PDI moieties (1.2 nm). According to the molecular model, there is an alternating longitudinal shift between two adjacent π-stacked PDI molecules. The overall periodic motif obtained from FFT (2.1 nm) is in

good agreement with the molecular model (2.1 nm). Photonic properties of 1 are consistent with highly ordered structure (see below).

TEM imaging of an air-dried sample of compound 1 did not achieve sufficient contrast to observe crystalline order, however, it was observed for dried assemblies of 2 and 3 (see below).

Compound 2 self-assembles in water at pH 10 (see Methods section for the preparation procedure) to give ordered structures similar to the ones formed by compound 1. Cryo-TEM shows formation of highly ordered arrays, and FFT analysis of the cryo-TEM images exhibits well-defined spots corresponding to a spacing of 2.1 nm (Figure 3A). Dark-contrast (1.1 ± 0.2-nm wide) and light-contrast stripes (0.9 ± 0.3 nm) correspond well to the width of PDI core stacks (1.1 nm) and ethyl propyl interaction areas (0.9 nm), respectively, in the molecular model of a crystalline monolayer (Figure 3B). In addition, high-contrast structures having width of approximately 2.5 nm were observed in cryo-TEM (yellow arrows, Figure 3A), most probably corresponding to cross sections of the 2D assemblies oriented near-perpendicular to the vitrified water layer in cryo-TEM (the width of the stacked aromatic core of 2 according to the molecular model is ∼2 nm). Photonic properties of 2 are consistent with highly ordered structure (see below). The crystalline-like structure of the assemblies is preserved upon drying as evidenced by TEM images of 2 cast from aqueous solutions (Supporting Information Figure S4).

Compound 3 was assembled in water/THF solutions since it is not soluble in pure water. Cryo-TEM imaging of compound 3 in water/THF (1:1, v/v) revealed highly ordered film-like assemblies, presenting a crystalline-like structure constructed by high contrast stripes (1.2 ± 0.2 nm) and low contrast ones
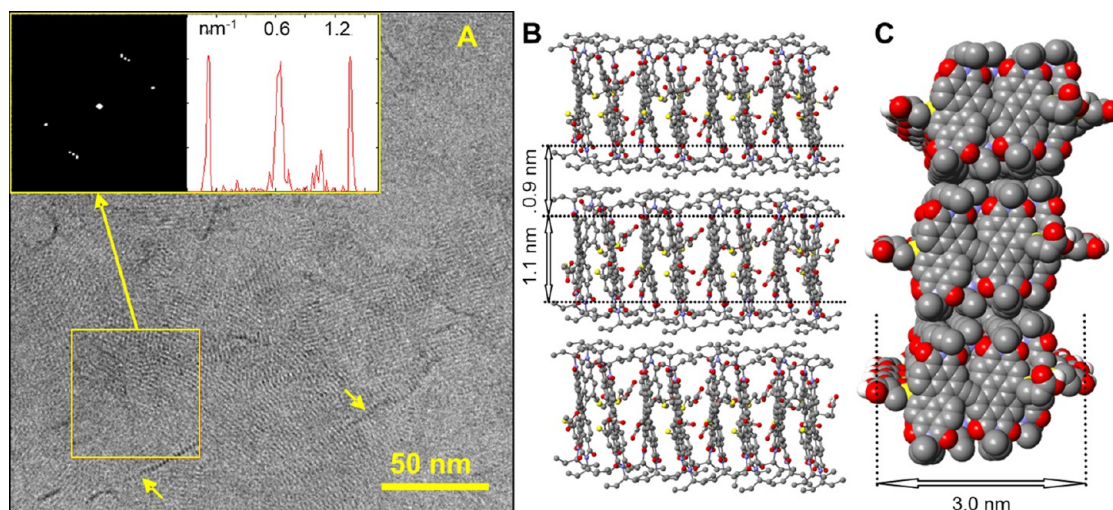
Figure 3. (A) cryo-TEM image of 1×10^{-4} M solution of 2 in water (pH 10). Inset: FFT analysis of the marked area. Yellow arrows point to high contrast structures corresponding to the monolayer cross section. (B,C) Molecular model (hydrogens are omitted for clarity): (B) interacting stacks and dimensions corresponding to the dark and light contrast stripes in the assemblies; (C) side view (space filling representation) showing the width of the assembly (monolayer cross section).

(0.8 ± 0.3 nm). According to the molecular model, the size of the PDI aromatic unit (N—N distance) is 1.2 nm and the inter-stack distance which contains the ethyl-propyl groups attached to the imide nitrogen is 0.8 nm (Figure 4B), both in good agreement with the cryo-TEM image analysis data (1.2 ± 0.2 and 0.8 ± 0.3 nm). FFT analysis of the cryo-TEM images gave rise to a spacing of 2.2 nm (Figure 4A), corresponding well to the molecular model. High-contrast structures having width of approximately 3 nm were observed in cryo-TEM (yellow arrows, Figure 4A), corresponding to cross sections of the 2D assemblies oriented near-perpendicular to the vitrified water layer in cryo-TEM, matching the width of the stacked aromatic core of **3** according the molecular model (3 nm). The structure is preserved upon drying as evidenced by TEM images of **3** cast from aqueous solutions (Figure S5). We note that the formation of highly ordered structures assembled from **3** was observed in cryo-TEM also in the presence of lower THF content (Figure S7).

AFM measurements of the assemblies of **1**−**3** deposited on a Si wafer were employed (see Supporting Information for details) in order to probe the monolayer thickness (Figure 5). The air-dried samples of **1** deposited from water gave rise to flat assemblies extending over several micrometers with a height (thickness) of 1.5 ± 0.2 nm (Figure 5A), corresponding to the oxygen−oxygen distance (between terminal carboxyls) of 1.7 nm (Figure 2C). AFM measurements of **2** revealed relatively flat assemblies having height (thickness) of 3.1 ± 0.3 nm (Figure 5B), which corresponds well to the monolayer width in the molecular model (3 nm, Figure 3C). AFM images of compound **3** on a Si wafer revealed film-like assemblies (Figure 5C). The films are flat and present sharp and well-defined edges. The height of a layer was 4.3 ± 0.5 nm. The overall height

of the layer including contribution of the PEG chains upon drying should be 6.2 nm (see Supporting Information for details). However, the pressure under the AFM tip compresses the loose PEG groups so that they contribute only partially to the observed height of monomolecular layers (see Supporting Information for calculations). Evidently, the thickness of the 2D nanosheets is defined by the size of a molecular building block. Notably, overall morphology and order are largely retained upon deposition and drying of the dissolved assemblies.

Remarkably, the systems possessing different hydrophilic/hydrophobic ratio (**1** and **2**) are capable of forming crystalline arrays at the same conditions (10^{-4} M water solution at pH 10). This underscores the dominance of "aromatic stack/aliphatic edge motif" (Figure 1) in aqueous medium, leading to the ordered energetically favorable structures assembled from different molecular units, and under various conditions. Provided the stacking/hydrophobic interactions between the aromatic cores are dominant and the system is equilibrated, aromatic bolaamphiphiles bearing alkyl groups should have a propensity to assemble into ordered 2D arrays.

Photophysical Studies. UV−vis spectra indicate that the assemblies based on **1**−**3** in aqueous medium show significant red shifts and absorption band broadening (Figure 6) in comparison with molecularly dissolved systems. Compound **1** in water gives rise to a broad absorption centered at 576 nm, significantly red-shifted from the one of a molecularly dissolved system in chloroform (peaking at 528 nm). Compounds **2** and **3** show broadened absorption peaks in aqueous media, concomitant with development of new red-shifted bands peaking at 615 and 667 nm for compound **2**, and 643 and 702 nm for compound **3**. No change was observed in the UV−vis spectra of aqueous solutions of **1**−**3** upon aging. UV−vis spectra of films deposited on
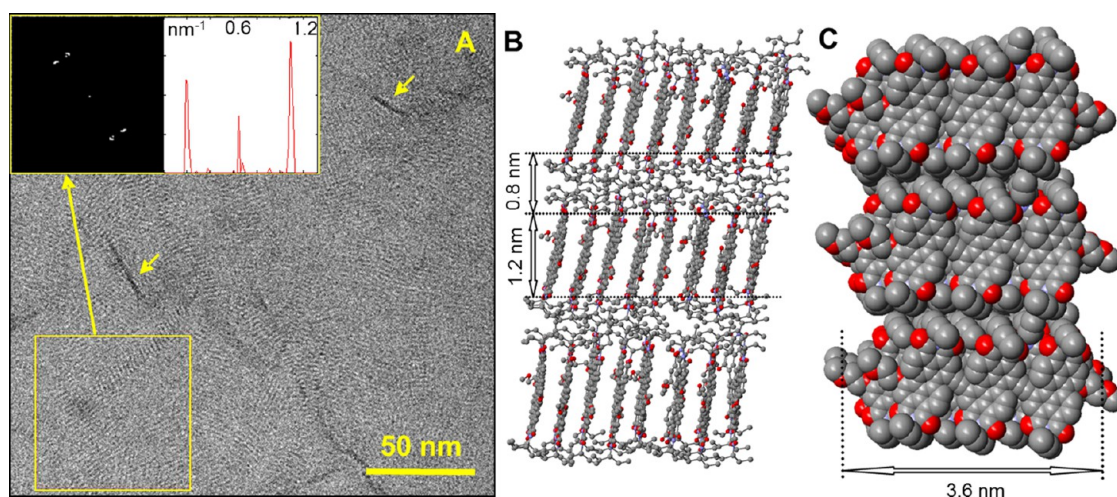
Figure 4. (A) cryo-TEM image of 1×10^{-4} M solution of 3 in 1:1 THF/water (v/v). Inset: FFT analysis of the marked area. Yellow arrows point to high contrast areas corresponding to the monolayer cross section. (B,C) Molecular model (hydrogens are omitted for clarity, PEGs are modeled as $-OCH_2CH_2OCH_3$): (B) interacting stacks and dimensions corresponding to the dark and light contrast stripes in the assemblies; (C) side view (space filling representation) showing the width of the assembly (monolayer cross section). The distance of 3.6 nm corresponds to O$-$O distance between the oxygens of $CH_2CH_2OCH_3$ groups (first PEG segment).
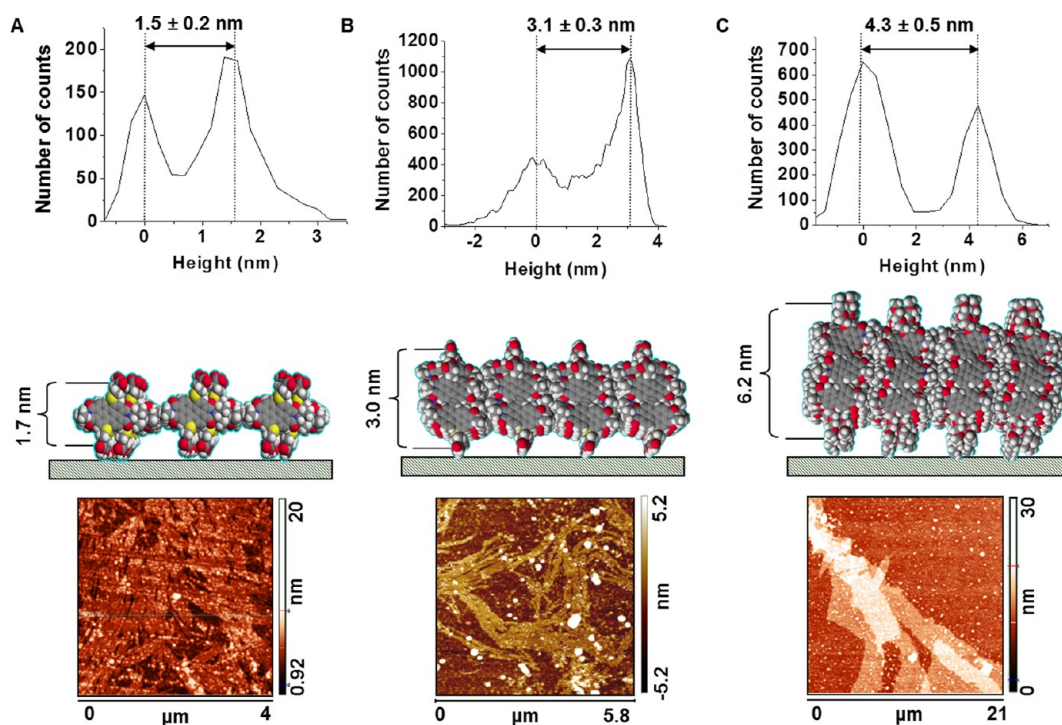

Figure 5. AFM measurements and histogram-height analysis of assemblies 1$-$3 (A$-$C, respectively). (Top) Histograms representing the height difference distribution of the air-dried film on Si surface (in panel C, the height difference portrayed is between substrate and the first layer of the material). (Middle) Molecular models of 1$-$3 demonstrate a good correlation to the measured film width. (Bottom) AFM images. Small mounds of material appearing as bright spots on the films were avoided in height analysis. The AFM image in C shows a second layer on top of parts of the first.

quartz slides from aqueous solution are similar to those observed for the aqueous assemblies (especially in the case of **1** and **2**, Figure 6). Emission is almost completely quenched in aqueous solutions of **1**$-$**3**.

Our observations are in agreement with the broadening and red shifts of UV$-$vis absorption bands observed in the absorption spectra from PDI crystals,[38$-$40] liquid crystals,[41] and other ordered arrays,[42,43] due to

formation of a band structure arising from specific interactions between the stacked PDI π-systems.[40,44$-$46] According to our modeling that fits best to the cryo-TEM data, in the assemblies of **1** there is a longitudinal shift between the PDI cores (J-aggregation, Figure 2), and in the case of **2** and **3**, slight longitudinal and transverse shifts are observed (Figures 3 and 4), which arise from interaction modes imposed by multi-PDI
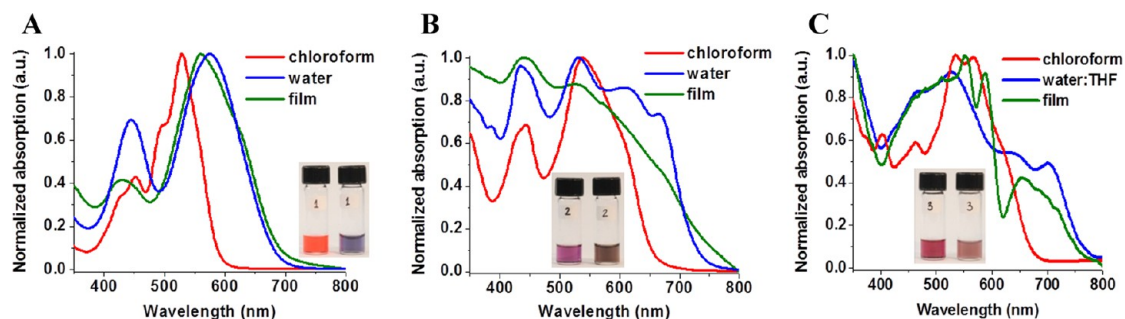
Figure 6. UV−vis spectra of compounds **1**−**3** in aggregated (aqueous media) and disaggregated (chloroform) state compared with the air-dried films deposited from aqueous solutions: (A) **1**; (B) **2**; (C) **3** (water/THF = 1:1). Insets: photographs of **1**−**3** in disaggregating (chloroform, left) and aggregating (aqueous media, right) solvents (1×10^{-4} M).
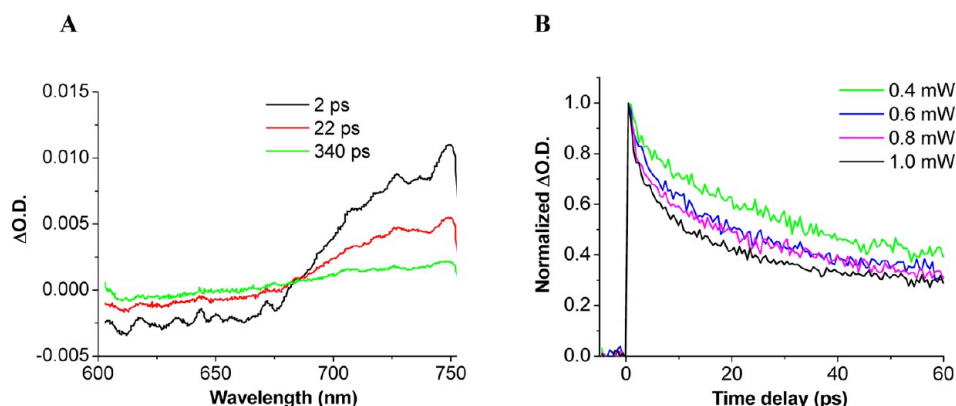
Figure 7. Transient absorption of **2** (10^{-4} M water solution, pH 10, 48 h aging). (A) Representative transient spectra; (B) decay kinetics (probed at 745 nm, normalized, initial 60 ps decay) at different laser powers.

cores (see Supporting Information Figure S8). These interaction modes are consistent with the observed red shifts in ordered systems.[40,44]

Concerning light harvesting, assemblies **1**−**3** show excellent solar spectrum coverage (Figure 6), with absorption extending to 800 nm in the case of **2** and **3**, while strong electronic coupling between the chromophore units and long-range order may result in efficient excitation energy transfer. To investigate the excited state dynamics, we performed femtosecond transient absorption (fsTA) studies on **1**−**3** in their molecular and assembled states. The fsTA difference spectra of all systems show typical PDI excited state peaks (positive features in NIR region),[47] and corresponding PDI bleaching appears as broad negative features (Figure 7 and Supporting Information Figure S10). In the disaggregated state, the decay kinetics do not show a power dependence. In the case of ordered aqueous assemblies, the decay kinetics of **1** is power independent, while **2** and **3** exhibit strongly power dependent kinetics (Figure 7B, Supporting Information Figure S10, Table 1). The latter is indicative of exciton annihilation processes, typical of chromophore aggregates where a high photon flux leads to multiple excitations resulting in exciton annihilation due to efficient exciton diffusion.[11]

The kinetics of ordered arrays assembled from **1** was probed at 745 nm, with peak absorbance achieved within 1.5 ps, followed by decay with a time constant of ∼20 ps (Supporting Information Figure S9). Presence of a rise time together with power independence may indicate formation of more complex exciton states that are self-trapped. The reason for such exciton behavior is not clear at present and will represent a subject of future studies.

The kinetics of crystalline assemblies of **2** and **3** exhibit a fast decay component that is dependent on the laser power (Figure 8 and Supporting Information Figure S10). To estimate exciton diffusion coefficient and diffusion length, we used an analysis method, in which the data obtained at different laser powers were fitted using the bimolecular annihilation rate equation:[15,48]

$$\frac{d}{dt} n(t) = -\frac{n(t)}{\tau} - \gamma(t)n(t)^2 \qquad (1)$$

where $n(t)$ is the exciton population at time t, τ is the intrinsic lifetime of an exciton (when no annihilation takes place) and $\gamma(t)$ is the annihilation rate. Within this framework, we utilized one-dimensional diffusion model for the annihilation rate:[15,48]
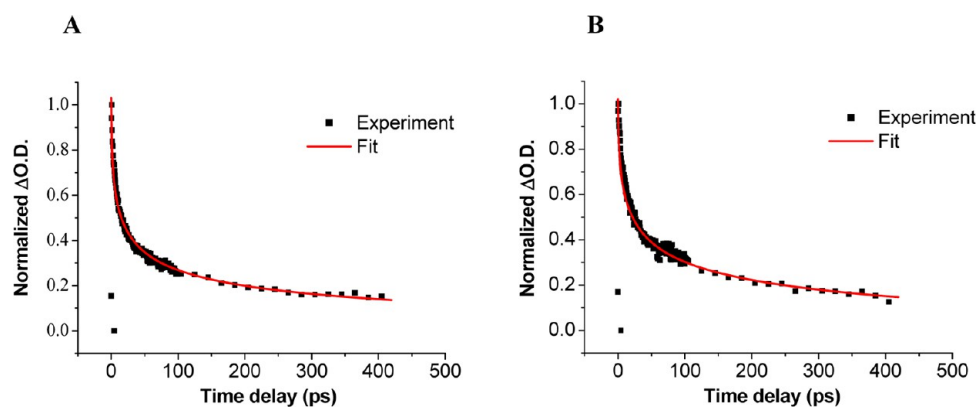
A

B

Figure 8. Fit (using the solution of eq 1 and 2, see Supporting Information for details) of the decay kinetics of crystalline arrays assembled from compound **2** (10^{-4} M water solution, pH 10, 48 h aging) measured at different laser excitation powers: (A) 1.0 mW; (B) 0.6 mW.

TABLE 1. Diffusion Coefficient and Exciton Diffusion Length for Assemblies 2 and 3

	D, cm²/s	$L_D{}^a$, nm
2	0.078 ± 0.020	120 ± 10
3	0.016 ± 0.005	35 ± 10

^{a} Exciton diffusion length is calculated using $L_D = (D\tau)^{1/2}$, where τ is the exciton lifetime (estimated as a longer decay component of the decay fit, representing a lower limit for the exciton lifetime).

$$\gamma_{1D}(t) = \frac{1}{aN_0}\sqrt{\frac{4D}{\pi t}} \qquad (2)$$

where a is the 1D lattice constant (distance between the adjacent molecules in the stack, 3.4 Å), D is the exciton diffusion constant, and N_0 is the molecular density (number of molecules in the assembly per unit volume). This model fits best our data, which is in accordance with previous works,[16,49] revealing that exciton diffusion occurs primarily within 1D aromatic stacks because of strong electronic coupling within the stacks and weaker interstack coupling. Fitting to the experimental data is presented in Figure 8 and Supporting Information Figure S11, and the exciton diffusion parameters are given in Table 1.

The diffusion coefficient in the case of **3** is comparable to that found for solution-phase PDI J-aggregates (1.3×10^{-2} cm²/s).[49] Notably, the diffusion coefficient in the case of **2** (7.8×10^{-2} cm²/s) is even slightly higher than the 4×10^{-2} cm²/s value reported for PTCDA (perylene tetracarboxylic dianhydride) crystalline films.[16] Exciton diffusion lengths are comparable to those found for PTCDA films (61 nm)[16] and PDI

J-aggregates (96 nm, from exciton annihilation study,[49] and 70 nm from fluorescence blinking study[50]). Thus, extended solution-phase crystalline nanosheets assembled from **2** and **3** exhibit excellent solar spectrum coverage and fast exciton diffusion, representing advantageous light-harvesting systems that can efficiently collect and deliver excitons over large areas using nanometer-thick material.

CONCLUSIONS

We have designed a family of amphiphilic PDI derivatives that self-assemble into crystalline 2D structures in aqueous solutions. This assembly motif is generated by hierarchical mode of two distinct hydrophobic interaction types induced by an aromatic core and alkyl groups, suggesting a simple design strategy to obtain crystalline organic assemblies in water. The self-assembled materials largely preserve their ordered structure in the dry state. Assemblies based on **2** and **3** show promising light-harvesting characteristics, with **2** exhibiting exciton diffusion comparable to solid crystalline films. The light absorption properties, ordered 2D morphology and nanoscale thickness of the nanosheets appear to be useful for fabrication of light-harvesting systems. Remarkably, relatively simple molecular systems can be designed to undergo self-assembly into extended ordered assemblies with advantageous photonic properties using water as an assembling medium. The ability to rationally design and efficiently assemble aromatic crystalline systems in aqueous media may lead to water-based photonic and electronic materials employing facile, cost-efficient, and environmentally friendly fabrication and processing.

METHODS

Preparation of the Assemblies. Samples of compound **1** were prepared by dissolving the dry material in double-distilled water (Barnstead NANOpure Diamond water system, used

for all sample preparations) containing 2 equiv of NaOH. Clear homogeneous blue solutions were obtained and aged for at least one day, longer aging did not result in significant changes in sample appearance and morphologies as evidenced by UV−vis absorption measurements and by

cryo-TEM imaging. pH was adjusted by using HCl or NaOH solutions.

Samples of **2** were prepared by dissolving the dry material in THF followed by the injection of the THF solution into double-distilled water containing 2 equivalents of NaOH and subsequent evaporation of the THF cosolvent, followed by addition of water and pH adjustment to pH 10 using NaOH solution. Clear homogeneous brown solutions were obtained and aged for 8 days. The absence of THF is verified by ^{1}H NMR (in D_2O).

The samples of **3** were prepared by dissolving the dry material in THF followed by adding water to reach THF:water=1:1 (volume ratio) and 5 min sonication. The resulted assembly was then aged for 3 days at room temperature. Clear homogeneous brown solutions were obtained.

Transmission Electron Microscopy. Imaging was performed using Tecnai T12 transmission electron microscope operated at 120 kV.

Sample-Preparation. A total of 2.5 μL of each sample was applied to 400-mesh copper grid coated with carbon (on nitrocellulose support) that was pretreated by glow discharge (60 s).

Cryo-Transmission Electron Microscopy. Imaging was performed using a Tecnai F20 transmission electron microscope operating at 200 kV, and using a Gatan 626 cooling holder and transfer station with a Gatan US4000 CCD digital camera, or a Tecnai T12 transmission electron microscope operated at 120 kV, using a Gatan 626 cooling holder and transfer station, with a TVIPS F244HD CCD digital camera.

Sample Preparation. Eight microliters of each sample was applied to a 300-mesh copper grid coated with holey carbon (Pacific Grid-Tech supplies). The samples were blotted at 25 °C and 95% relative humidity, and plunged into liquid ethane using Leica EM-GP Automatic Grid Plunger. Specimens were equilibrated at −178 °C in the microscope prior to the imaging process.

AFM Measurements. *Sample Preparation.* AFM measurements were carried out on a (100) Si wafer substrate with 200 nm oxide. Ten microliters of 1×10^{-4} M of each solution was incubated on a 1×1 cm^2 die of Si for 1 min before blotting the excess liquid and drying under a dry nitrogen stream to avoid formation of stacked deposits of the film upon drying. AFM measurements were made using either a MMAFM instrument equipped with an E-scanner (Bruker-nano, Santa Barbara, CA) or with an NTEGRA equipped with SF005 head and 10 μm^2 scanner (NT-MDT, Zelenograd). Scans were made in tapping/semicontact mode using an AC240 TS silicon probe (Olympus).

Heights of the film structures were determined using individual cross sections and histogram height analysis. For the latter, most probable pixel heights over a region containing primarily background with minimal amount of debris were subtracted from average heights of regions encompassing a single layer of the assembly films.

Femtosecond Transient Absorption. Spectroscopy was performed using a system based on a modelocked Ti:sapphire oscillator (Spectra Physics MaiTai). The oscillator produces a train of <120-fs pulses (bandwidth ∼10 nm fwhm), with a peak wavelength centered at 800 nm. The weak oscillator pulses are amplified by a chirped pulse regenerative amplifier (CPA) (Spectra Physics Spitfire ACE). The pulses are first stretched, then regeneratively amplified in a Ti:sapphire cavity, pumped by a pulsed Nd:YLF laser (Spectra Physics Empower 45) operating at 1 kHz. After the pulse has been amplified and recompressed, its energy is about 5.0 mJ in a train of 1-kHz pulses, and about 1 mJ is used in the transient absorption setup. An independent pump pulse is obtained by pumping an optical parametric amplifier (Spectra Physics OPA-800CF) that produces 120-fs pulses tunable from 300 nm to 3 μm. The output power of the OPA is a few microjoules (depending on the chosen wavelength) at 1 kHz. The pump beam is mechanically chopped at half the amplifier repetition rate. The chopper (C-995 TTI) is synchronized with the Spitfire pulses. Normally a few thousand pulse pairs (pump on/pump off) are averaged to produce a transient absorption spectrum with a noise level below 0.3 mOD. A small portion of the remaining amplified pulse is used to generate a white light continuum as a probe pulse. To this end, the Ti:Sapphire beam is focused onto a 3-mm thick sapphire disk by a 10-cm focal length lens, and the numerical aperture of the beam is controlled by an iris placed in front of the lens to obtain a stable and smooth white light continuum. The resulting beam is passed through a Raman notch filter in order to remove the remains of the 800 nm fundamental beam from the probe white light continuum. The pump and probe pulses are crossed in the sample at a small angle, while maintaining a magic angle between the pump and probe polarizations. The remains of the pump pulse are removed by passing the probe through an iris, and it is then imaged onto an optical fiber that brings it into a fiber optic interface, which focuses the light onto the entrance slit of a Jobin Yvon Triax 180 spectrograph. The light is normally dispersed by a 300 g/mm grating onto a fast CCD camera (Andor Newton DU-970N−UV, operating at 1000 spectra/s using "crop mode'). The whole setup is controlled by National Instruments LabView software. A variable neutral-density filter was employed to adjust the pump power for studying the power dependence. The pump power intensities were measured using an Ophir powermeter with a photodiode sensor in proximity to the sample. The excitation densities were calculated for a laser spot of 300 μm diameter on the sample. This diameter was measured by placing beamprofiler (Ophir Beamstar FX33) at the sample position and determining the 4-σ (95% of the power) parameter. In the reported experiments, the pump was turned to 525 or to 590 nm and the optical densities of the samples (in 4 mm and 2 mm optical path length cuvettes) were kept between 0.2 and 0.5 at the excitation wavelength. The instrument response function (300 fs) was recorded by repetition of the experiments with sample replaced by pure solvent and keeping all other parameters unchanged. Spectral corrections and analysis were performed using Surface Xplorer Pro (Ultrafast Systems) and Origin 7.5 (OriginLab) software.

Conflict of Interest: The authors declare no competing financial interest.

Supporting Information Available: Synthesis and characterization of **1**−**3**, TEM images, and transient absorption data. This material is available free of charge *via* the Internet at http://pubs.acs.org.

REFERENCES AND NOTES

1. Oshovsky, G. V.; Reinhoudt, D. N.; Verboom, W. Supramolecular Chemistry in Water. *Angew. Chem., Int. Ed.* **2007**, *46*, 2366–2393.
2. Holder, S. J.; Sommerdijk, N. A. J. M. New Micellar Morphologies from Amphiphilic Block Copolymers: Disks, Toroids and Bicontinuous Micelles. *Polym. Chem.* **2011**, *2*, 1018–1028.
3. Rybtchinski, B. Adaptive Supramolecular Nanomaterials Based on Strong Noncovalent Interactions. *ACS Nano* **2011**, *5*, 6791–6818.
4. Spicer, P. T. Progress in Liquid Crystalline Dispersions: Cubosomes. *Curr. Opin. Colloid Interface Sci.* **2005**, *10*, 274–279.
5. Rosen, B. M.; Wilson, C. J.; Wilson, D. A.; Peterca, M.; Imam, M. R.; Percec, V. Dendron-Mediated Self-Assembly, Disassembly, and Self-Organization of Complex Systems. *Chem. Rev.* **2009**, *109*, 6275–6540.
6. Ryu, J. H.; Hong, D. J.; Lee, M. Aqueous Self-Assembly of Aromatic Rod Building Blocks. *Chem. Commun.* **2008**, 1043–1054.

7. Rehm, T. H.; Schmuck, C. Ion-Pair Induced Self-Assembly in Aqueous Solvents. *Chem. Soc. Rev.* **2010**, *39*, 3597–3611.

8. Percec, V.; Wilson, D. A.; Leowanawat, P.; Wilson, C. J.; Hughes, A. D.; Kaucher, M. S.; Hammer, D. A.; Levine, D. H.; Kim, A. J.; Bates, F. S.; et al. Self-Assembly of Janus Dendrimers into Uniform Dendrimersomes and Other Complex Architectures. *Science* **2010**, *328*, 1009–1014.

9. Gustafsson, J.; LjusbergWahren, H.; Almgren, M.; Larsson, K. Cubic Lipid-Water Phase Dispersed into Submicron Particles. *Langmuir* **1996**, *12*, 4611–4613.

10. Peterca, M.; Percec, V.; Leowanawat, P.; Bertin, A. Predicting the Size and Properties of Dendrimersomes from the Lamellar Structure of Their Amphiphilic Janus Dendrimers. *J. Am. Chem. Soc.* **2011**, *133*, 20507–20520.

11. Pope, M.; Swenberg, C. E. *Electronic Processes in Organic Crystals and Polymers*; Oxford University Press: New York, 1999.

12. Zhan, X. W.; Facchetti, A.; Barlow, S.; Marks, T. J.; Ratner, M. A.; Wasielewski, M. R.; Marder, S. R. Rylene and Related Diimides for Organic Electronics. *Adv. Mater.* **2011**, *23*, 268–284.

13. Lunt, R. R.; Benziger, J. B.; Forrest, S. R. Relationship between Crystalline Order and Exciton Diffusion Length in Molecular Organic Semiconductors. *Adv. Mater.* **2010**, *22*, 1233–1236.

14. Najafov, H.; Lee, B.; Zhou, Q.; Feldman, L. C.; Podzorov, V. Observation of Long-Range Exciton Diffusion in Highly Ordered Organic Semiconductors. *Nat. Mater.* **2010**, *9*, 938–943.

15. Inoue, A.; Yoshihar, K.; Nagakura, S. Exciton-Exciton Interaction and Exciton Migration in Anthracene, Pyrene, and Perylene Crystals. *Bull. Chem. Soc. Jpn.* **1972**, *45*, 1973–1976.

16. Engel, E.; Leo, K.; Hoffmann, M. Ultrafast Relaxation and Exciton-Exciton Annihilation in PTCDA Thin Films at High Excitation Densities. *Chem. Phys.* **2006**, *325*, 170–177.

17. Nelson, J. Organic Photovoltaic Films. *Curr. Opin. Solid State Mater. Sci.* **2002**, *6*, 87–95.

18. Walter, M. G.; Rudine, A. B.; Wamser, C. C. Porphyrins and Phthalocyanines in Solar Photovoltaic Cells. *J. Porphyrins Phthalocyanines* **2010**, *14*, 759–792.

19. Scholes, G. D.; Fleming, G. R.; Olaya-Castro, A.; van Grondelle, R. Lessons from Nature About Solar Light Harvesting. *Nat. Chem.* **2011**, *3*, 763–774.

20. Wasielewski, M. R. Self-Assembly Strategies for Integrating Light Harvesting and Charge Separation in Artificial Photosynthetic Systems. *Acc. Chem. Res.* **2009**, *42*, 1910–1921.

21. Würthner, F.; Kaiser, T. E.; Saha-Moller, C. R. J-Aggregates: From Serendipitous Discovery to Supramolecular Engineering of Functional Dye Materials. *Angew. Chem., Int. Ed.* **2011**, *50*, 3376–3410.

22. Abbel, R.; Schenning, A. P. H. J.; Meijer, E. W. Fluorene-Based Materials and Their Supramolecular Properties. *J. Polym. Sci., Part A: Polym. Chem.* **2009**, *47*, 4215–4233.

23. Desiraju, G. R. Crystal Engineering: A Brief Overview. *J. Chem. Sci.* **2010**, *122*, 667–675.

24. De Yoreo, J. J.; Vekilov, P. G. Principles of Crystal Nucleation and Growth. *Rev. Mineral Geochem.* **2003**, *54*, 57–93.

25. Weissbuch, I.; Lahav, M.; Leiserowitz, L. Toward Stereochentical Control, Monitoring, and Understanding of Crystal Nucleation. *Cryst. Growth Des.* **2003**, *3*, 125–150.

26. Hill, J. P.; Jin, W.; Kosaka, A.; Fukushima, T.; Ichihara, H.; Shimomura, T.; Ito, K.; Hashizume, T.; Ishii, N.; Aida, T. Self-Assembled Hexa-Peri-Hexabenzocoronene Graphitic Nanotube. *Science* **2004**, *304*, 1481–1483.

27. Baram, J.; Shirman, E.; Ben-Shitrit, N.; Ustinov, A.; Weissman, H.; Pinkas, I.; Wolf, S. G.; Rybtchinski, B. Control over Self-Assembly through Reversible Charging of the Aromatic Building Blocks in Photofunctional Supramolecular Fibers. *J. Am. Chem. Soc.* **2008**, *130*, 14966–14967.

28. Golubkov, G.; Weissman, H.; Shirman, E.; Wolf, S. G.; Pinkas, I.; Rybtchinski, B. Economical Design in Noncovalent Nanoscale Synthesis: Diverse Photofunctional Nanostructures Based on a Single Covalent Building Block. *Angew. Chem., Int. Ed.* **2009**, *48*, 926–930.

29. Krieg, E.; Shirman, E.; Weissman, H.; Shimoni, E.; Wolf, S. G.; Pinkas, I.; Rybtchinski, B. Supramolecular Gel Based on a Perylene Diimide Dye: Multiple Stimuli Responsiveness, Robustness, and Photofunction. *J. Am. Chem. Soc.* **2009**, *131*, 14365–14373.

30. Nam, K. T.; Shelby, S. A.; Choi, P. H.; Marciel, A. B.; Chen, R.; Tan, L.; Chu, T. K.; Mesch, R. A.; Lee, B. C.; Connolly, M. D. Free-Floating Ultrathin Two-Dimensional Crystals from Sequence-Specific Peptoid Polymers. *Nat. Mater.* **2010**, *9*, 454–460.

31. Brustolin, F.; Goldoni, F.; Meijer, E. W.; Sommerdijk, N. A. J. M. Highly Ordered Structures of Amphiphilic Polythiophenes in Aqueous Media. *Macromolecules* **2002**, *35*, 1054–1059.

32. Görl, D.; Zhang, X.; Würthner, F. Molecular Assemblies of Perylene Bisimide Dyes in Water. *Angew. Chem., Int. Ed.* **2012**, *51*, 6328–6348.

33. Zhang, X.; Rehm, S.; Safont-Sempere, M. M.; Würthner, F. Vesicular Perylene Dye Nanocapsules as Supramolecular Fluorescent Ph Sensor Systems. *Nat. Chem.* **2009**, *1*, 623–629.

34. Krieg, E.; Weissman, H.; Shirman, E.; Shimoni, E.; Rybtchinski, B. A Recyclable Supramolecular Membrane for Size-Selective Separation of Nanoparticles. *Nat. Nanotechnol.* **2011**, *6*, 141–146.

35. Backes, C.; Hauke, F.; Hirsch, A. The Potential of Perylene Bisimide Derivatives for the Solubilization of Carbon Nanotubes and Graphene. *Adv. Mater.* **2011**, *23*, 2588–2601.

36. Ehli, C.; Oelsner, C.; Guldi, D. M.; Mateo-Alonso, A.; Prato, M.; Schmidt, C.; Backes, C.; Hauke, F.; Hirsch, A. Manipulating Single-Wall Carbon Nanotubes by Chemical Doping and Charge Transfer with Perylene Dyes. *Nat. Chem.* **2009**, *1*, 243–249.

37. Englert, J. M.; Rohrl, J.; Schmidt, C. D.; Graupner, R.; Hundhausen, M.; Hauke, F.; Hirsch, A. Soluble Graphene: Generation of Aqueous Graphene Solutions Aided by a Perylenebisimide-Based Bolaamphiphile. *Adv. Mater.* **2009**, *21*, 4265–4269.

38. Zang, L.; Che, Y. K.; Moore, J. S. One-Dimensional Self-Assembly of Planar Π-Conjugated Molecules: Adaptable Building Blocks for Organic Nanodevices. *Acc. Chem. Res.* **2008**, *41*, 1596–1608.

39. Klebe, G.; Graser, F.; Haedicke, E.; Berndt, J. Crystallochromy as a Solid-State Effect: Correlation of Molecular Conformation, Crystal Packing and Color in Perylene-3,4:9,10-Bis(Dicarboximide) Pigments. *Acta Crystallogr., Sect. B: Struct. Sci.* **1989**, *B45*, 69–77.

40. Kazmaier, P. M.; Hoffmann, R. A Theoretical-Study of Crystallochromy—Quantum Interference Effects in the Spectra of Perylene Pigments. *J. Am. Chem. Soc.* **1994**, *116*, 9684–9691.

41. Cormier, R. A.; Gregg, B. A. Synthesis and Characterization of Liquid Crystalline Perylene Diimides. *Chem. Mater.* **1998**, *10*, 1309–1319.

42. Würthner, F.; Bauer, C.; Stepanenko, V.; Yagai, S. A Black Perylene Bisimide Super Gelator with an Unexpected J-Type Absorption Band. *Adv. Mater.* **2008**, *20*, 1695–1698.

43. Gallaher, J. K.; Aitken, E. J.; Keyzers, R. A.; Hodgkiss, J. M. Controlled Aggregation of Peptide-Substituted Perylene-Bisimides. *Chem. Commun.* **2012**, *48*, 7961–7963.

44. Delgado, M. C. R.; Kim, E. G.; da Silva, D. A.; Bredas, J. L. Tuning the Charge-Transport Parameters of Perylene Diimide Single Crystals via End and/or Core Functionalization: A Density Functional Theory Investigation. *J. Am. Chem. Soc.* **2010**, *132*, 3375–3387.

45. Fink, R. F.; Seibt, J.; Engel, V.; Renz, M.; Kaupp, M.; Lochbrunner, S.; Zhao, H. M.; Pfister, J.; Würthner, F.; Engels, B. Exciton Trapping in Pi-Conjugated Materials: A Quantum-Chemistry-Based Protocol Applied to Perylene Bisimide Dye Aggregates. *J. Am. Chem. Soc.* **2008**, *130*, 12858–12859.

46. Gisslen, L.; Scholz, R. Crystallochromy of Perylene Pigments: Interference between Frenkel Excitons and Charge-Transfer States. *Phys. Rev. B* **2009**, *80*.

47. Wasielewski, M. R. Energy, Charge, and Spin Transport in Molecules and Self-Assembled Nanostructures Inspired by Photosynthesis. *J. Org. Chem.* **2006**, *71*, 5051–5066.

48. Suna, A. Kinematics of Exciton-Exciton Annihilation in Molecular Crystals. *Phys. Rev. B* **1970**, *1*, 1716–1739.

49. Marciniak, H.; Li, X. Q.; Würthner, F.; Lochbrunner, S. One-Dimensional Exciton Diffusion in Perylene Bisimide Aggregates. *J. Phys. Chem. A* **2011**, *115*, 648–654.

50. Lin, H. Z.; Camacho, R.; Tian, Y. X.; Kaiser, T. E.; Würthner, F.; Scheblykin, I. G. Collective Fluorescence Blinking in Linear J-Aggregates Assisted by Long-Distance Exciton Migration. *Nano Lett.* **2010**, *10*, 620–626.